


New level scheme and shell model description of ^{212}Rn

C. B. Li (李聪博),¹ G. L. Zhang (张高龙) ^{2,3,*}, C. X. Yuan (袁岑溪),⁴ G. X. Zhang (张广鑫),^{5,6} S. P. Hu (胡世鹏),⁷ W. W. Qu (屈卫卫),⁸ Y. Zheng (郑云),¹ H. Q. Zhang (张焕乔),¹ D. Mengoni,^{5,6} D. Testov,^{5,6} J. J. Valiente-Dobón,⁹ H. B. Sun (孙慧斌),⁷ N. Wang (王楠),⁷ X. G. Wu (吴晓光),¹ G. S. Li (李广生),¹ M. Mazzocco,^{5,6} A. Gozzelino,⁹ C. Parascandolo,¹⁰ D. Pierroutsakou,¹⁰ M. La Commara,^{10,11} F. Recchia,^{5,6} A. I. Sison,⁹ S. Bakes,⁹ I. Zanon,⁹ S. Aydin,¹² and D. Bazzacco^{5,6}

¹China Institute of Atomic Energy, Beijing 102413, China

²School of Physics, Beihang University, Beijing 100191, China

³Beijing Advanced Innovation Center for Big Data-Based Precision Medicine, School of Medicine and Engineering, Beihang University, Beijing, 100191, China

and Key Laboratory of Big Data-Based Precision Medicine (Beihang University),

Ministry of Industry and Information Technology, Beijing 100191, China

⁴Sino-French Institute of Nuclear Engineering and Technology, Sun Yat-Sen University, Zhuhai 519082, China

⁵Dipartimento di Fisica e Astronomia dell'Università di Padova, I-35131 Padova, Italy

⁶Istituto Nazionale di Fisica Nucleare, Sezione di Padova, I-35131 Padova, Italy

⁷College of Physics and Optoelectronic Engineering, Shenzhen University, Shenzhen 518060, China

⁸School of Radiation Medicine and Protection, Medical College of Soochow University, Soochow 215123, China

⁹INFN, Laboratori Nazionali di Legnaro, I-35020 Legnaro, Italy

¹⁰INFN-Sezione di Napoli, via Cintia, I-80126 Napoli, Italy

¹¹Dipartimento di Farmacia, Università di Napoli "Federico II", via D. Montesano, I-80131 Napoli, Italy

¹²Department of Physics, University of Aksaray, 68100 Aksaray, Turkey



(Received 28 November 2019; accepted 24 March 2020; published 20 April 2020)

Level structures of ^{212}Rn have been studied by in-beam γ -ray spectroscopic methods using the $^{209}\text{Bi}(^6\text{Li}, 3n)^{212}\text{Rn}$ reaction at beam energies of 28, 30, and 34 MeV. A number of new nonyrast states based on $\pi h_{9/2}^4$ and $\pi h_{9/2}^3 f_{7/2}$ configurations have been identified. A 3^{-} collective state is also proposed at 2121 keV, which is most likely formed by mixing the octupole vibration with the 3^{-} member of the $\pi h_{9/2}^3 i_{13/2}$ multiplet. The level scheme is compared with large-scale shell model calculations and discussed in terms of excitations of valence protons and without contributions from the ^{208}Pb core. An overall excellent agreement is obtained for states that can be described in this model space.

DOI: [10.1103/PhysRevC.101.044313](https://doi.org/10.1103/PhysRevC.101.044313)

I. INTRODUCTION

For many years, the spherical nuclei near the doubly closed shell nucleus $^{208}\text{Pb}_{126}$ have provided a laboratory in the heavy-element region in which the large-scale shell model had been confronted by experiment [1,2]. Therefore, it is particularly important to have complete experimental data in this mass region. A large amount of information on nuclei near ^{208}Pb has been obtained through a wide variety of experiments. Nevertheless, there are many gaps in the data.

The nucleus ^{212}Rn , with its relatively simple structure of a closed neutron core, has four valence protons outside the doubly closed shell ^{208}Pb core, provides a convenient system of nuclei for testing the study of both low- and high-spin states, and has received much attention in the past few decades. The first study [3,4] of the high-spin level structure of ^{212}Rn used the $^{204}\text{Hg}(^{13}\text{C}, 5n)^{212}\text{Rn}$ reaction to establish the basic structure of the nucleus to an excitation energy of about

8.5 MeV, some involving double neutron core excitations. Afterwards, a number of isomers and high-lying γ -ray transitions were observed [5–7]. Recently, Dracoulis *et al.* [8,9], using the $^{204}\text{Hg}(^{13}\text{C}, 5n)^{212}\text{Rn}$ and the $^{198}\text{Pt}(^{18}\text{O}, 4n)^{212}\text{Rn}$ reactions, extended the level scheme to higher spin ($39\hbar$), with an excitation energy in excess of 13 MeV, covering states formed by aligned valence protons combined with single, double, and triple neutron-core excitations. These were interpreted in terms of both the empirical shell model (ESM) and the deformed independent particle model (DIPM). Lifetimes, g -factors and magnetic moments were also measured by different groups and interpreted them in terms of diverse microcosmic model [4,10–13,15]. To sum up, previous studies of the in-beam γ -ray spectroscopy have provided some details on the energies and decay characteristics of intermediate-high spin states in ^{212}Rn . However, these studies have produced no information at all about the levels of $\pi h_{9/2}^2 f_{7/2}^2$ configuration, for the $\pi h_{9/2}^3 f_{7/2}$ and $\pi h_{9/2}^3 i_{13/2}$ configurations with $J \leq 6$, the data are inadequate or nonexistent, and particularly there is absence of the extremely interesting collective 3^{-} state. Therefore, much more low-lying information is needed about

*zgl@buaa.edu.cn

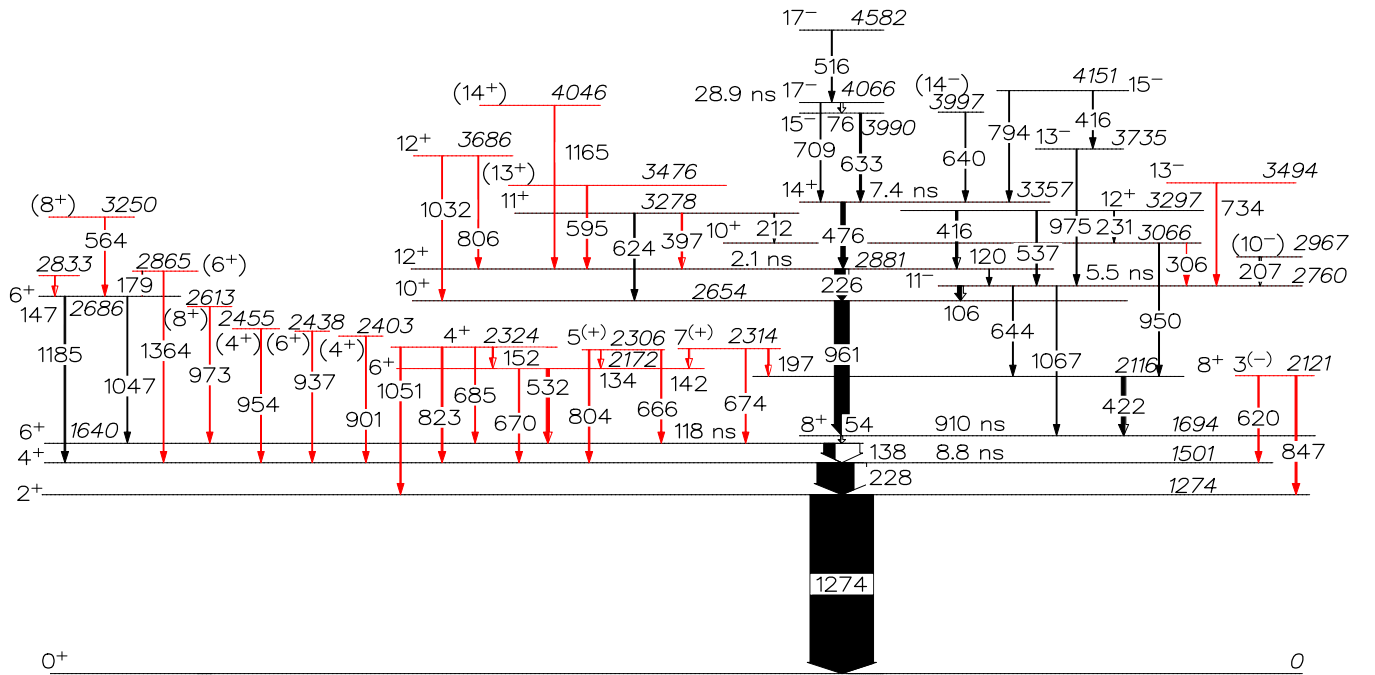


FIG. 1. Partial level scheme of ^{212}Rn in the present work. Newly assigned levels and γ transitions are marked by red color. The arrow widths are approximately proportional to the relative γ -ray intensities, while the white part of the arrows is the correction due to internal conversion [14]. The evaluated half-lives in Ref. [15] for the isomeric states are also indicated.

γ -decay properties, which are a sensitive probe of the wave functions.

The experimental results reported in this paper were obtained in the course of a study of reaction mechanisms induced by weakly bound nucleus ^6Li on ^{209}Bi target, the details of which will be described in a future paper. The level scheme established as a result of the present investigation differs in several important aspects from that of previous work. The reaction $^{209}\text{Bi}(^6\text{Li}, 3n)^{212}\text{Rn}$, with beam energies of 28, 30, and 34 MeV in the present work, would result in a more favored population of nonyrast states than found in previous heavy-ion experiments, more side-feeding into the 2^+ , 4^+ , and 6^+ states. In addition, large-scale shell model (SM) calculations were performed in the full $Z = 82$ –126 proton model space $\pi(0h_{9/2}, 1f_{7/2}, 0i_{13/2}, 2p_{3/2}, 1f_{5/2}, 2p_{1/2})$ to interpret new level scheme.

II. EXPERIMENT AND RESULT

The experiment was performed at the Tandem-XTU accelerator of Legnaro National Laboratory in Italy. The target consisted of a $500 \mu\text{g}/\text{cm}^2$ ^{209}Bi backed with a $100 \mu\text{g}/\text{cm}^2$ C foil. The de-excitation γ rays from the reaction residues were detected with the GALILEO γ -ray array which is made of 25 Compton-Suppressed bismuth germanate high-purity germanium (BGO-HPGe) detectors distributed on four rings: ten detectors at 90° and five detectors at each of the angles 119° , 129° , and 152° . The relative photo peak efficiencies of detector array and energy calibrations were performed using ^{60}Co , ^{137}Cs , ^{152}Eu , and ^{133}Ba standard radioactive sources.

A total of 8.4×10^9 γ - γ two and higher-fold coincidence events were recorded. The data were sorted into symmetrized

and angular correlation γ - γ matrices for off-line analysis. An asymmetric angular correlation matrix between the detectors at 152° and at 90° was constructed and used for the directional correlation of oriented states (DCO) ratio analysis to distinguish between quadrupole and dipole transitions. In our array geometry, a DCO ratio of about 1.0 is expected if the gating and the observed transition are stretched transitions of pure and equal multipole order. $R_{\text{DCO}} \approx 0.6$ is expected for a pure dipole transition gated on a stretched quadrupole transition. Spin and parity assignments are based upon previously reported data, our DCO measurements, systematic considerations and shell model calculations. Unbracketed assignments in Fig. 1 indicate the highly probably assignments, while more speculative spin assignments are indicated in parentheses.

In the present experiment, the light-mass beam preferred exiting more low-spin nonyrast states, so no higher spin states information is established. The previously reported level schemes below $17\hbar$ are for the most part confirmed, and about 29 new γ transitions and 16 new levels are placed in the intermediate-low spins of the level scheme. In particular, several unplaced γ rays from very early decay works [15] are assigned. Table I lists all transitions assigned to ^{212}Rn with their energies, intensities, DCO ratios, and assignments into the level scheme.

Coincidence measurements and sum-difference relationships among γ -ray energies have been used to construct the level scheme shown in Fig. 1. The coincidence spectra gated on the 1273.7 and 227.6 keV [Figs. 2(a) and 2(b)] show transitions which precede in time the decay of the 8^+ isomer, provide an overview of the γ transitions placed in ^{212}Rn . The 228 keV γ peak is double. The transition energy (226.3 keV in this case) is also observed in coincidence with the 961 keV

TABLE I. Level excitation energy E_x , energies E_γ , relative intensities, DCO ratios, initial- and final-state spin-parities, and multipolarities of γ -ray transitions assigned to ^{212}Rn in the present work.

E_x (keV)	E_γ (keV)	I_γ	R_{DCO}^a	$I_i^\pi \rightarrow I_f^\pi$	Mult.
1273.7	1273.7(1)	100(4.5)	0.93(6)	$2^+ \rightarrow 0^+$	$E2$
1501.3	227.6(1)	58.8(47)	1.04(7)	$4^+ \rightarrow 2^+$	$E2$
1639.5	138.2(1)	17.6(20)	1.06(8)	$6^+ \rightarrow 4^+$	$E2$
1693.7	54.2 ^b			$8^+ \rightarrow 6^+$	$E2$
2115.7	422.0(1)	4.3(7)	1.27(24)	$8^+ \rightarrow 8^+$	$E2$
2121.0	847.3(1)	2.3(3)	0.76(14)	$3^{(-)} \rightarrow 2^+$	($E1$)
	619.5(2)	0.5(1)	0.65(15)	$3^{(-)} \rightarrow 4^+$	($E1$)
2171.7	670.4(1)	1.1(2)	0.99(16)	$6^+ \rightarrow 4^+$	$E2$
	532.2(1)	3.4(5)	1.11(20)	$6^+ \rightarrow 6^+$	$E2$
2305.6	804.3(1)	1.7(4)	0.71(14)	$5^{(+)} \rightarrow 4^+$	($M1/E2$)
	666.0(3)	0.3(1)	0.75(18)	$5^{(+)} \rightarrow 6^+$	($M1/E2$)
	133.7(2)	<0.1		$5^{(+)} \rightarrow 6^+$	($M1/E2$)
2313.5	674.0(2)	0.3(1)	0.69(14)	$7^{(+)} \rightarrow 6^+$	($M1/E2$)
	197.3(2)	1.2(1)	0.75(18)	$7^{(+)} \rightarrow 8^+$	($M1/E2$)
	141.8(2)	<0.1		$7^{(+)} \rightarrow 6^+$	($M1/E2$)
2324.3	1050.9(4)	0.4(1)	1.11(19)	$4^+ \rightarrow 2^+$	$E2$
	823.0(2)	1.2(2)	1.01(17)	$4^+ \rightarrow 4^+$	$E2$
	684.9(2)	0.5(1)	1.12(26)	$4^+ \rightarrow 6^+$	$E2$
	152.4(2)	<0.1		$4^+ \rightarrow 6^+$	$E2$
2402.7	901.4(2)	1.1(2)	0.96(23)	$(4^+) \rightarrow 4^+$	($E2$)
2437.8	936.5(2)	0.3(1)	1.12(38)	$(6^+) \rightarrow 4^+$	($E2$)
2455.3	954.0(2)	0.4(1)	1.02(22)	$(4^+) \rightarrow 4^+$	($E2$)
2612.9	973.4(2)	0.5(1)	1.08(29)	$(8^+) \rightarrow 6^+$	($E2$)
2654.5	960.8(1)	23(2)	1.09(13)	$10^+ \rightarrow 8^+$	$E2$
2686.2	1046.6(2)	0.4(1)	0.94(22)	$6^+ \rightarrow 6^+$	$E2$
	1184.9(1)	1.9(2)	1.15(15)	$6^+ \rightarrow 4^+$	$E2$
2760.3	105.8(1)	5.3(4)	0.67(8)	$11^- \rightarrow 10^+$	$E1$
	644.4(5)	<0.1		$11^- \rightarrow 8^+$	$E3$
	1067.1(3)	0.2(1)		$11^- \rightarrow 8^+$	$E3$
2833.3	147.1(2)	<0.1			
2865.4	1364.0(3)	0.3(1)	1.15(25)	$(6^+) \rightarrow 4^+$	($E2$)
	179.2(2)	0.2(1)		$(6^+) \rightarrow (6^+)$	($E2$)
2880.8	226.3(1)	13(1)	1.04(18)	$12^+ \rightarrow 10^+$	$E2$
	120.3(2)	<0.1		$12^+ \rightarrow 11^-$	$E1$
2966.8	206.5(1)	1.0(1)	0.66(8)	$(10^-) \rightarrow 11^-$	($E1$)
3065.5	949.9(1)	2.3(2)	0.91(11)	$10^+ \rightarrow 8^+$	$E2$
	305.5(2)	0.4(1)	0.70(13)	$10^+ \rightarrow 11^-$	$E1$
3250.3	564.1(2)	0.4(1)	0.97(31)	$(8^+) \rightarrow (6^+)$	($E2$)
3278.0	623.5(2)	1.5(2)	0.65(23)	$11^+ \rightarrow 10^+$	$M1/E2$
	396.6(2)	1.3(2)	0.64(21)	$11^+ \rightarrow 12^+$	$M1/E2$
	212.1(2)	0.3(2)	0.59(25)	$11^+ \rightarrow 10^+$	$M1/E2$
3296.9	536.6(1)	1.6(3)	0.65(11)	$12^+ \rightarrow 11^-$	$E1$
	231.4(2)	0.2(1)	1.14(26)	$12^+ \rightarrow 10^+$	$E2$
	416.4(1)	2.2(2)	1.01(18)	$12^+ \rightarrow 12^+$	$E2$
3357.0	476.2 (1)	6.1(7)	0.97(11)	$14^+ \rightarrow 12^+$	$E2$
3475.9	595.1(2)	1.5(3)	0.61(13)	$(13^+) \rightarrow 12^+$	($E1$)
3493.9	733.6(2)	0.4(1)	1.21(40)	$13^- \rightarrow 11^-$	$E2$
3686.4	1031.9(2)	0.4(1)	1.11(28)	$12^+ \rightarrow 10^+$	$E2$
	806.1(2)	0.8(1)	1.16(26)	$12^+ \rightarrow 12^+$	$E2$
3735.0	974.7(2)	1.2(2)	0.96(22)	$13^- \rightarrow 11^-$	$E2$
3990.3	633.3(2)	2.7(3)	0.56(17)	$15^- \rightarrow 14^+$	$E1$
3997.3	640.3(2)	1.0(1)	1.11(17)	$(14^-) \rightarrow 14^+$	($E1$)
4045.7	1164.9(2)	0.5(1)	1.08(20)	$(14^+) \rightarrow 14^+$	($E2$)
4065.9	75.6(5)			$17^- \rightarrow 15^-$	$E2$
	708.7(2)	0.7(2)	0.45(18)	$17^- \rightarrow 14^+$	$E3$

TABLE I. (Continued.)

E_x (keV)	E_γ (keV)	I_γ	R_{DCO}^a	$I_i^\pi \rightarrow I_f^\pi$	Mult.
4150.7	793.7(2)	0.5(1)	0.59(18)	$15^- \rightarrow 14^+$	$E1$
	415.5(2)	<0.1		$15^- \rightarrow 13^-$	$E2$
4581.5	515.6(2)	0.6(1)	0.94(16)	$17^- \rightarrow 17^-$	$E2$

^aFrom the known quadrupole transition DCO gate.

^bNot observed in this work. This transition is from previous work [15].

above the 8^+ isomer state. No prompt coincidences are, of course, observed through the 910 ns isomer state [15]. The 54-keV γ ray was not observed directly partly because its intensity would be low (since it was a highly converted $E2$ transition) and partly because the efficiency of detectors is very low at the low-energy region.

The EC-decay experiments and the heavy-ion in-beam studies have identified all even-spin low-lying yrast states, and only a tentative proposal for the secondary 6^+ state could be made from the decay data, based on two linking γ transitions, the 1185 keV γ ray to the 4_1^+ level, and the 1047 keV one to the 6_1^+ level. We also see γ transitions of the 1185 and 1047 keV and both transitions have $\Delta I = 2$ or $\Delta I = 0$ character. Thus, we adopt $J = 6^+$ for the level at 2686 keV. Three new (147, 179, and 564 keV) γ transitions are found to feed this state and tentatively placed on the level scheme. No DCO information can be obtained for 147 and 179 keV γ transitions. Except for 179 keV γ transition, the

level at 2865 keV is also de-excited by a $\Delta I = 2$ 1364 keV γ transition to the 4_1^+ state, we propose $J = 6^+$ for this level. For the 2833 keV level no spin-parity information can be obtained.

Five new levels at 2121, 2172, 2306, 2314, and 2324 keV are fixed based on their more decay paths, respectively. Previously, the 532, 620, 670, and 823 keV γ rays were observed in the ^{212}Fr decay work, however, they were not placed in level scheme; while 804 keV γ ray was tentatively attributed to depopulation of a level at 2306 keV [15]. Our work observed that the level at 2121 keV depopulate by 847 and 620 keV γ transitions to the 2_1^+ and 4_1^+ levels; the level at 2172 keV depopulates by the 670 and 532 keV γ transitions to the 4_1^+ and 6_1^+ levels; the level at 2306 keV depopulates by the 804 and 666 keV γ transitions to the 4_1^+ and 6_1^+ levels; and the level at 2324 keV depopulates by the 685, 823, and 1051 keV γ transitions to the 6_1^+ , 4_1^+ , and 2_1^+ levels. We were able to observe two additional depopulating γ rays supported by γ - γ coincidences. The 134 and 152 keV

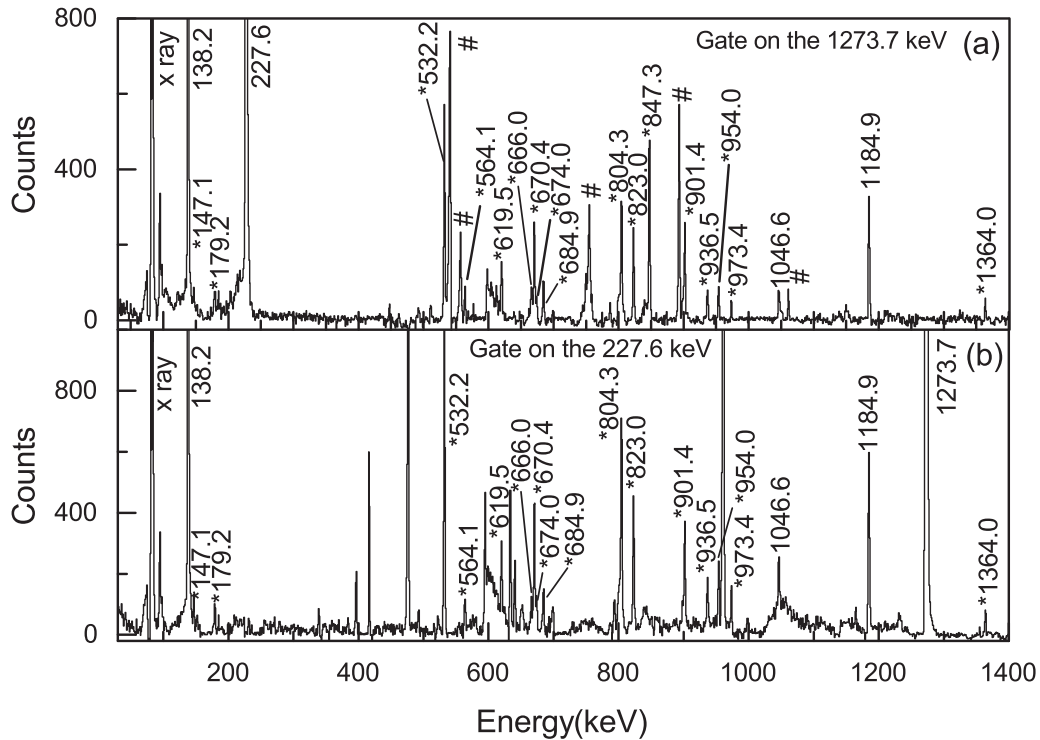


FIG. 2. γ -ray coincidence spectra for ^{212}Rn gated (a) on the 1273.7 keV, (b) 227.6 keV transition. The 227.6 keV ($4^+ \rightarrow 2^+$) peak partially overlaps that of the 226.3 keV ($12^+ \rightarrow 10^+$) peak. Nevertheless, due to the long lifetime of the $J = 8^+$ isomer, one can obtain very good separation of the two 227 keV components. The contaminants from double 227 keV transition above the 8^+ isomer are not labeled, only those peaks common to the (a, b) two-component spectra are labeled in (b). γ rays marked with asterisks are newly assigned transitions. Contaminants from other nuclei are indicated by #.

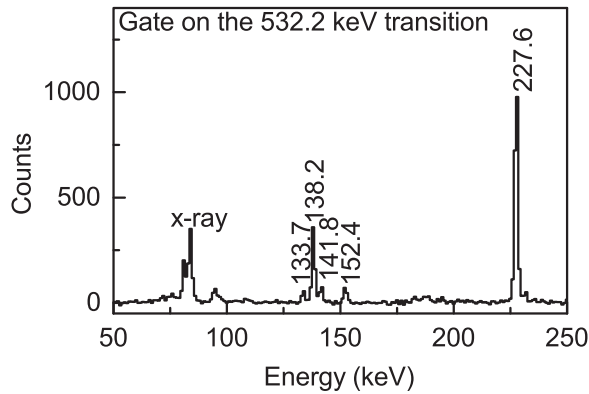


FIG. 3. γ -ray coincidence spectrum for ^{212}Rn gated on the 532.2 keV transition.

γ transitions are, respectively, placed between the 2306 and 2172 keV levels and between the 2324 and 2172 keV levels on the basis of coincidences with the 532 and 670 keV γ rays that depopulates the 2172 keV level (see the 532.2 keV gated spectrum in Fig. 3). The 532, 670, 685, and 823 keV γ transitions have $\Delta I = 2$ or $\Delta I = 0$ character. Therefore, for the states at 2172 and 2324 keV spin 4 or 6 is possible. For 2324 keV state, spin-parity is assigned as 4^+ due to observing the 1151 keV γ transitions to the 2_1^+ state. For the lower 2172 keV state, its spin-parity cannot be 4^+ , because of its link to the 2314 keV level ($J = 7$, which will be discussed subsequently) by means of the 142 keV γ transition. We thus adopt $J^\pi = 6^+$ for the level at 2172 keV. In addition, a new state at 2314 keV depopulated both of the below and above the 8^+ isomer is also identified, which depopulates by 674, 197, and 142 keV γ transitions to the 6_1^+ , 8_2^+ , and 6_2^+ levels. All of the 197, 620, 666, 674, 804, 823, and 847 keV γ transitions have $\Delta I = 1$ character. Thus, the spin at 2121 keV level is determined to be 3, the spin at 2306 keV level is determined to be 5, and the spin at 2314 keV level is 7. The 1^+ , 2^+ , and 3^+ states are as a rule very weakly populated in the ($^6\text{Li}, xn$) reactions, contrary to the correspondingly intensities what were observed for 847 and 620 keV γ transitions. Thus, the 2121 keV level is most likely the 3^- collective candidate state analogous to that observed in ^{208}Pb , ^{210}Po , and ^{216}Th [16]. In the neighboring even-even ^{210}Po isotone, the 5^+ and 7^+ states with configurations $\pi h_{9/2}f_{7/2}$ were observed at near degeneracy above the 8_2^+ state with stretched $\pi h_{9/2}f_{7/2}$ configuration. Meanwhile, the 5^+ state in ^{210}Po was observed to decay via four paths to 4_1^+ , 6_1^+ , 4_2^+ , and 6_2^+ levels; while the 7^+ state was observed to decay via four paths to 6_1^+ , 8_1^+ , 6_2^+ , and 8_2^+ levels [17]. Based on systematics, we conclude that the near degeneracy 2306 and 2314 levels in ^{212}Rn are most likely the corresponding 5^+ and 7^+ states. The suggested $5^{(+)}$ level seems to be well established with transitions to the 4_1^+ , 6_1^+ , and 6_2^+ states; the suggested $7^{(+)}$ level seems to be also well established with transitions to the 6_1^+ , 8_2^+ , and 6_2^+ states. One more remark, in ^{210}Po isotone four odd-spin 1^+ , 3^+ , 5^+ , and 7^+ yrast states are near degeneracy and the 1^+ , 3^+ , 5^+ , and 7^+ states in ^{212}Rn are also predicted to be near degeneracy with energies of 2317, 2366, 2354, and 2299 keV (shell model calculations in the next section), respectively. On the basis

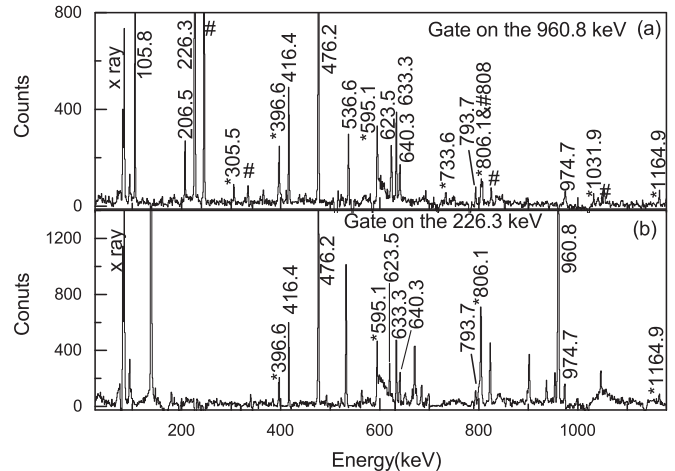


FIG. 4. γ -ray coincidence spectra for ^{212}Rn gated (a) on the 960.8 keV, (b) 226.3 keV transition. The same as described in the caption of Fig. 2, due to the long lifetime of the $J = 8^+$ isomer, one can obtain very good separation of the two 227 keV components. Only those lines common to the two-component spectra are labeled, the contaminants from double 228 keV transition below the 8^+ isomer are not labeled in (b). γ rays marked with asterisks are newly assigned transitions. Contaminants are indicated by #.

of level systematics and theoretical predictions, the parity of $J = 3$ state at 2121 keV level is very unlikely to be positive. This further supports the $3^{(-)}$ assignment of 2121 keV level mentioned above.

In addition, four new levels at 2403, 2438, 2455, and 2613 keV are only defined by a single transition to the yrast state below the 8^+ isomer state. All of them have $\Delta I = 2$ or $\Delta I = 0$ character, thus the spins of 2403, 2438, and 2455 keV levels are limited probably to be 4 or 6, while the spin of 2613 keV is limited probably to be 6 or 8. In Fig. 1, tentative spin assignments of these four levels are indicated in parentheses.

The new γ transitions and previously assigned γ transitions above the 8^+ isomer state are also clearly displayed in the coincidence spectra gated on the 960.8 and 226.3 keV γ transitions, respectively [Figs. 4(a) and 4(b)]. Two levels (3476 and 4046 keV) were tentatively placed on the level scheme and one level (3686 keV) is fixed based on associated 1032 and 806 keV depopulating γ transitions. Both of 1032 and 806 keV γ transitions have $\Delta I = 2$ or $\Delta I = 0$ character, and thus 12^+ is adopted for 3686 keV level. The level at 2967 keV was observed in Ref. [5] with a single decay (207 keV) to the 11^- yrast state, but no spin-parity assignment was given. Recent work of Dracoulis *et al.* [9] could not assign this state either. In the present experiment we find a strong population of this state. It has a $\Delta I = 1$ character. The systematics of Rn isotopes [18] found that in ^{206}Rn the 10^- state was 110 keV below the 11^- state and in ^{208}Rn these states were very close together, while in ^{210}Rn and ^{212}Rn the 10^- state was not observed and was inferred that the 10^- and 11^- states swap positions. Thus, here we arbitrarily adopted (10^-) as the probable spin-parity for this state. Our shell-model calculations also predict that the $\pi h_{9/2}^3 i_{13/2}$ 10^- state lies above the 11^- state from the same configuration in

next section. In addition, two new γ transitions (306 keV and 397 keV) are found linking the previously known levels.

III. DISCUSSION

The present work firstly identifies the 5^+ and 7^+ odd-spin yrast states, more nonyrast states for the 4^+ , 6^+ , and 8^+ states, and possible collective 3^- state. In the following discussion we will compare the experimental data for these levels with shell model calculations. The calculations are performed in the full $Z = 82-126$ proton model space $\pi(0h_{9/2}, 1f_{7/2}, 1f_{5/2}, 2p_{3/2}, 2p_{1/2}, 0i_{13/2})$. The two-body matrix elements of the Hamiltonian are from KHPE [19,20]. The single particle energies of the Hamiltonian are fixed to be the single particle levels of ^{209}Bi . Contributions from the neutron orbitals and other proton orbitals were not considered. Similar calculations for the $N = 126$ isotopes have been performed in Refs. [21,22]. Although the used Hamiltonian is slightly different from the present one, the results agree with each other.

The experimental and theoretical spectra of ^{212}Rn are compared in Fig. 5 and the configurations of the levels are presented in Table II. ^{212}Rn , with its four valence protons, is obvious that the $0h_{9/2}$, $1f_{7/2}$, and $0i_{13/2}$ orbits are important in the description of low-lying states. The negative-parity states have in common active particles in the $0i_{13/2}$ intruder orbital. Here all the experimental spins up to present observed $17^- \hbar$ are reported, while higher-spins states have been observed and their description is likely to require that core-excited states be explicitly taken into account, and is not expected to be adequately reproduced within our model space.

From Fig. 5 we see that the calculated spectrum reproduces very well the experimental one. The calculated states which are shown in Fig. 5 and Table II are all the 36 states arising from the configurations $\pi h_{9/2}^4$, $\pi h_{9/2}^3 f_{7/2}$, $\pi h_{9/2}^3 i_{13/2}$, $\pi h_{9/2}^2 f_{7/2}^2$, and $\pi h_{9/2}^2 f_{7/2} i_{13/2}$. Several tentative levels were placed on the level scheme, as mentioned above, we have tried to establish correspondence with calculated levels. In Fig. 5 we see that the calculated spectrum is mainly characterized by three groups of configurations. The first group is the twelve numbers of levels dominated by the $\pi h_{9/2}^4$ configuration, while the second group contains the twelve members of the $\pi h_{9/2}^3 f_{7/2}$ multiplet. All negative-parity states, in addition to the 17^- state arising from the $\pi h_{9/2}^2 f_{7/2} i_{13/2}$ configuration, are in the third group dominated by the $\pi h_{9/2}^3 i_{13/2}$. The other two tentative states (6_5^+) and (14_2^+) suggested as $\pi h_{9/2}^2 f_{7/2}^2$ configuration are also placed on the third group. The percentage of the dominant configuration for all higher spin states is at least 90%, however, this is not the case for the lower-lying states, of which the wave functions contain significant configuration mixing, because these spins can be easily made up from a number of configurations. In the first four excited states the percentage of the dominant $\pi h_{9/2}^4$ configuration, ranges from 60% to 65% while it becomes 42% in the ground state. For other five low-lying excited states dominated by the $\pi h_{9/2}^3 f_{7/2}$ configuration, the percentages of the dominant configurations are about 70%. All the 12 levels arising from the $\pi h_{9/2}^4$ configuration have a configuration mixing with the $\pi h_{9/2}^2 i_{13/2}^2$ and $\pi h_{9/2}^2 f_{7/2}^2$ configurations in varying degrees. In fact, the

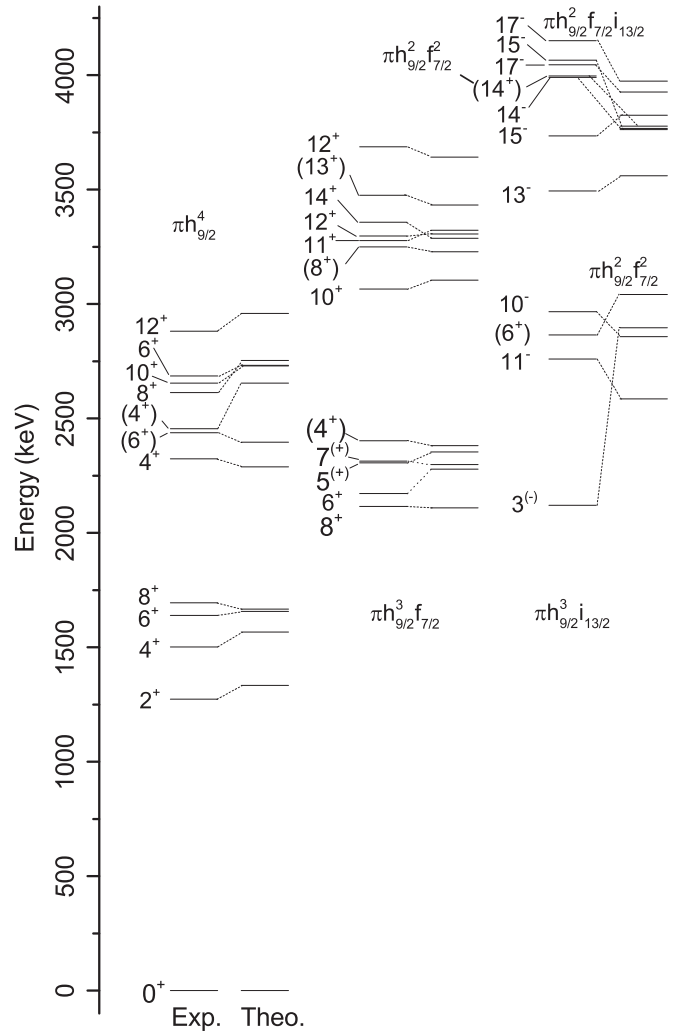


FIG. 5. A comparison between the experimentally observed levels in ^{212}Rn and those calculated (SM) as described in the text. The 6_5^+ , 14_2^+ , and 17_2^- levels, which are not assigned as the $\pi h_{9/2}^3 i_{13/2}$ configuration, are also shown on the right column, and labeled respectively. It should be noticed that the lowest 3^- states cannot be reproduced for obvious reasons, as the model space does not allow for excitations of the ^{208}Pb core, especially for neutron ph excitations.

percentages of latter configurations other than the mentioned above dominant one are 23% and 20% in the ground state, reducing to 3% and 2% in the 4_2^+ state. As well, all the 12 levels dominated by the $\pi h_{9/2}^3 f_{7/2}$ configuration have a significant mixing with $\pi h_{9/2} f_{7/2} i_{13/2}^2$ and $\pi h_{9/2} f_{7/2}^3$ configurations in low-lying states, until the 10_2^+ state is completely dominated by $\pi h_{9/2}^3 f_{7/2}$ (95%) multiplet. Similarity, the low-lying 10^- and 11^- dominated by $\pi h_{9/2}^3 i_{13/2}$ configuration have a significant mixing with $\pi h_{9/2} f_{7/2}^2 i_{13/2}$ and $\pi h_{9/2} i_{13/2}^3$ configurations. The 6_5^+ state contains 12% $\pi f_{7/2}^2 i_{13/2}^2$ and 8% $\pi h_{9/2}^3 f_{7/2}$ compositions.

The only experimental state for which we do not have a appropriate theoretical counterpart is the proposed $3^{(-)}$ state

TABLE II. Calculated (SM) multiparticle configurations in ^{212}Rn in the present work.

E_{exp} (keV)	J^π	E_{calc} (keV)	Configuration(%) ^a		
0	0^+	0	$\pi h_{9/2}^4$ (41.8%)	$\pi h_{9/2}^2 i_{13/2}^2$ (23.2%)	$\pi h_{9/2}^2 f_{7/2}^2$ (20.1%)
1274	2^+	1334	$\pi h_{9/2}^4$ (59.8%)	$\pi h_{9/2}^2 i_{13/2}^2$ (17.3%)	$\pi h_{9/2}^2 f_{7/2}^2$ (16.5%)
1501	4^+	1567	$\pi h_{9/2}^4$ (64.5%)	$\pi h_{9/2}^2 i_{13/2}^2$ (16.3%)	$\pi h_{9/2}^2 f_{7/2}^2$ (14.9%)
1640	6^+	1657	$\pi h_{9/2}^4$ (63.1%)	$\pi h_{9/2}^2 i_{13/2}^2$ (16.9%)	$\pi h_{9/2}^2 f_{7/2}^2$ (16.0%)
1694	8^+	1667	$\pi h_{9/2}^4$ (64.6%)	$\pi h_{9/2}^2 i_{13/2}^2$ (16.5%)	$\pi h_{9/2}^2 f_{7/2}^2$ (15.2%)
2116	8^+	2110	$\pi h_{9/2}^3 f_{7/2} i_{13/2}$ (70.7%)	$\pi h_{9/2} f_{7/2} i_{13/2}^2$ (15.1%)	$\pi h_{9/2} f_{7/2}^3$ (10.3%)
2121 ^b	3^-	2897	$\pi h_{9/2}^3 i_{13/2}$ (70.0%)	$\pi h_{9/2} i_{13/2}^3$ (12.5%)	$\pi h_{9/2} f_{7/2} i_{13/2}$ (11.8%)
2172	6^+	2278	$\pi h_{9/2}^3 f_{7/2} i_{13/2}$ (70.1%)	$\pi h_{9/2} f_{7/2} i_{13/2}^2$ (14.5%)	$\pi h_{9/2} f_{7/2}^3$ (9.7%)
2306	5^+	2354	$\pi h_{9/2}^3 f_{7/2} i_{13/2}$ (72.6%)	$\pi h_{9/2} f_{7/2} i_{13/2}^2$ (14.8%)	$\pi h_{9/2} f_{7/2}^3$ (9.2%)
2314	7^+	2299	$\pi h_{9/2}^3 f_{7/2} i_{13/2}$ (73.1%)	$\pi h_{9/2} f_{7/2} i_{13/2}^2$ (14.6%)	$\pi h_{9/2} f_{7/2}^3$ (9.0%)
2324	4^+	2288	$\pi h_{9/2}^3 i_{13/2}$ (89.3%)	$\pi h_{9/2}^2 i_{13/2}^2$ (2.7%)	$\pi h_{9/2}^2 f_{7/2}^2$ (2.3%)
2403	(4^+)	2381	$\pi h_{9/2}^3 f_{7/2} i_{13/2}$ (68.7%)	$\pi h_{9/2} f_{7/2} i_{13/2}^2$ (14.2%)	$\pi h_{9/2} f_{7/2}^3$ (9.5%)
2438	(6^+)	2396	$\pi h_{9/2}^3 i_{13/2}$ (91.2%)	$\pi h_{9/2}^2 i_{13/2}^2$ (2.4%)	$\pi h_{9/2}^2 f_{7/2}^2$ (1.8%)
2455	(4^+)	2654	$\pi h_{9/2}^3 i_{13/2}$ (94.0%)	$\pi h_{9/2}^2 i_{13/2}^2$ (1.7%)	$\pi h_{9/2}^2 f_{7/2}^2$ (1.6%)
2613	8^+	2754	$\pi h_{9/2}^3 i_{13/2}$ (95.2%)	$\pi h_{9/2}^2 i_{13/2}^2$ (1.5%)	$\pi h_{9/2}^2 f_{7/2}^2$ (1.4%)
2654	10^+	2732	$\pi h_{9/2}^3 i_{13/2}$ (94.6%)	$\pi h_{9/2}^2 i_{13/2}^2$ (1.7%)	$\pi h_{9/2}^2 f_{7/2}^2$ (1.4%)
2686	6^+	2730	$\pi h_{9/2}^3 i_{13/2}$ (95.1%)	$\pi h_{9/2}^2 i_{13/2}^2$ (1.5%)	$\pi h_{9/2}^2 f_{7/2}^2$ (1.3%)
2760	11^-	2585	$\pi h_{9/2}^3 i_{13/2}$ (70.7%)	$\pi h_{9/2} i_{13/2}^3$ (13.7%)	$\pi h_{9/2} f_{7/2}^2 i_{13/2}$ (12.5%)
2865	(6^+)	3042	$\pi h_{9/2}^3 f_{7/2} i_{13/2}$ (68.9%)	$\pi f_{7/2}^2 i_{13/2}^2$ (12.2%)	$\pi h_{9/2}^2 f_{7/2}^2$ (7.8%)
2881	12^+	2959	$\pi h_{9/2}^3 i_{13/2}$ (96.6%)	$\pi h_{9/2}^2 i_{13/2}^2$ (1.8%)	$\pi h_{9/2}^2 i_{13/2}^2$ (0.7%)
2967	(10^-)	2858	$\pi h_{9/2}^3 i_{13/2}$ (72.5%)	$\pi h_{9/2} i_{13/2}^3$ (12.6%)	$\pi h_{9/2} f_{7/2}^2 i_{13/2}$ (11.5%)
3066	10^+	3104	$\pi h_{9/2}^3 f_{7/2} i_{13/2}$ (95.4%)	$\pi h_{9/2} f_{7/2} i_{13/2}^2$ (1.1%)	$\pi h_{9/2}^2 i_{13/2}^2$ (0.9%)
3250	(8^+)	3228	$\pi h_{9/2}^3 f_{7/2} i_{13/2}$ (94.7%)	$\pi h_{9/2} f_{7/2} i_{13/2}^2$ (1.1%)	$\pi h_{9/2}^2 i_{13/2}^2$ (1.0%)
3278	11^+	3322	$\pi h_{9/2}^3 f_{7/2} i_{13/2}$ (98.2%)	$\pi h_{9/2}^2 i_{13/2}^2$ (0.8%)	$\pi h_{9/2} f_{7/2} i_{13/2}$ (0.3%)
3297	12^+	3306	$\pi h_{9/2}^3 f_{7/2} i_{13/2}$ (97.6%)	$\pi h_{9/2}^2 i_{13/2}^2$ (1.0%)	$\pi h_{9/2} f_{7/2} i_{13/2}$ (0.3%)
3357	14^+	3287	$\pi h_{9/2}^3 f_{7/2} i_{13/2}$ (98.5%)	$\pi h_{9/2}^2 i_{13/2}^2$ (1.0%)	$\pi h_{9/2}^2 f_{7/2}^2$ (0.3%)
3476	(13^+)	3433	$\pi h_{9/2}^3 f_{7/2} i_{13/2}$ (98.7%)	$\pi h_{9/2}^2 i_{13/2}^2$ (0.8%)	$\pi h_{9/2} f_{7/2}^2 i_{13/2}$ (0.2%)
3494	(13^-)	3561	$\pi h_{9/2}^3 i_{13/2}$ (96.4%)	$\pi h_{9/2} i_{13/2}^3$ (1.1%)	$\pi h_{9/2} f_{7/2}^2 i_{13/2}$ (0.9%)
3686	12^+	3642	$\pi h_{9/2}^3 f_{7/2} i_{13/2}$ (95.5%)	$\pi h_{9/2}^4$ (1.8%)	$\pi h_{9/2}^2 f_{7/2}^2$ (1.5%)
3735	13^-	3825	$\pi h_{9/2}^3 i_{13/2}$ (99.0%)	$\pi h_{9/2}^2 f_{7/2} i_{13/2}$ (0.2%)	$\pi h_{9/2} i_{13/2}^3$ (0.2%)
3990	15^-	3768	$\pi h_{9/2}^3 i_{13/2}$ (98.8%)	$\pi h_{9/2}^2 f_{5/2} i_{13/2}$ (0.3%)	$\pi h_{9/2} i_{13/2}^3$ (0.3%)
3997	14^-	3777	$\pi h_{9/2}^3 i_{13/2}$ (99.1%)	$\pi h_{9/2} i_{13/2}^3$ (0.2%)	$\pi h_{9/2} f_{7/2}^2 i_{13/2}$ (0.2%)
4046	(14^+)	3927	$\pi h_{9/2}^2 f_{7/2}^2$ (95.5%)	$\pi h_{9/2} f_{7/2} i_{13/2}^2$ (0.9%)	$\pi h_{9/2}^2 f_{7/2} f_{5/2}$ (0.8%)
4066	17^-	3762	$\pi h_{9/2}^3 i_{13/2}$ (99.6%)	$\pi h_{9/2} i_{13/2}^3$ (0.1%)	$\pi h_{9/2}^2 f_{7/2} i_{13/2}$ (0.1%)
4151	15^-	3974	$\pi h_{9/2}^3 i_{13/2}$ (98.6%)	$\pi h_{9/2}^2 f_{7/2} i_{13/2}$ (0.9%)	$\pi h_{9/2}^2 f_{5/2} i_{13/2}$ (0.2%)
4582	17^-	4374	$\pi h_{9/2}^2 f_{7/2} i_{13/2}$ (99.4%)	$\pi h_{9/2}^2 f_{7/2} i_{13/2}$ (0.4%)	$\pi h_{9/2} i_{13/2}^3$ (0.2%)

^aThe numbers are the probability (%) with which a given configuration is occupied. Only three maximal probabilities are given.

^bIt should be noticed that the lowest 3^- states cannot be reproduced for obvious reasons, as the model space does not allow for excitations of the ^{208}Pb core, especially for neutron ph excitations.

at 2121 keV. The octupole collective mode was well known in the heavy $Z \simeq 82$ and $N \simeq 126$ nuclei. It gives rise to the lowest excited state in ^{208}Pb , with energy of 2614 keV and spin-parity of 3^- . Moreover, the measurement of transition probability of $B(E3, 3^- \rightarrow 0^+) = 33.8(6)$ W.u. reveals its collective mode [17,23]. The structure of this octupole vibration comprises many coherent particle-hole excitations across the two magic gaps at $Z = 82$ and $N = 126$ involving several single-particle orbits with $\Delta l = 3$ ($\pi f_{7/2} - \pi i_{13/2}$ and $\nu g_{9/2} - \nu j_{15/2}$). In addition, one can expect that adding nucleon pairs to ^{208}Pb would result in a greater softness of the collective 3^- octupole mode, with a lowering of its energy well below 2614 keV. This was put forward in order to explain the behavior of the $E3$ strength in the $N = 127$ isotones, in the framework of particle-octupole vi-

bration coupling [24]. The evolution of the $3^- \rightarrow 0^+$ and $15/2^- \rightarrow 9/2^+$ excitation energies in the $N = 126$ and their neighboring odd- A $N = 127$ isotones are displayed in Fig. 6 as a function of Z . The excitation energy of 3^- in ^{212}Rn nicely accord with almost linearity decrease in energy when adding proton pairs similar to the case for $N = 127$ isotones. However, the calculations of present shell model locate the levels of the $\pi h_{9/2}^3 i_{13/2} 3^-$ proton multiplet at about 0.8 MeV above the corresponding possible level. This is more likely the result of some involved mixing the octupole vibration as in neighboring $N = 126$ ^{210}Po , ^{214}Ra , and ^{216}Th isotones [24]. Therefore, this state cannot be accounted for as they are intruders in the present model space. A systematic study of the influence of the number of valence particles on the 3^- energy will be interesting in future studies.

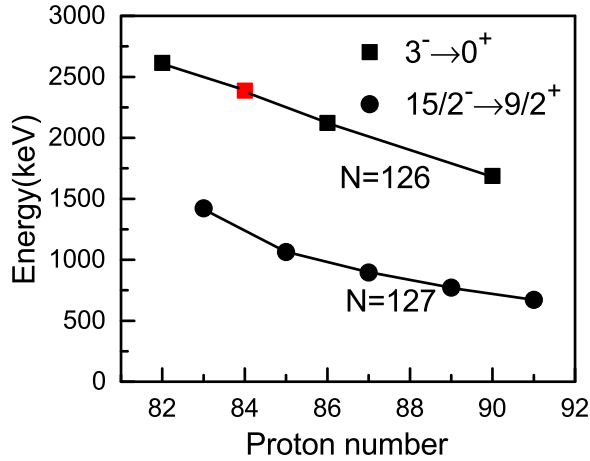


FIG. 6. The evolution of the $3^- \rightarrow 0^+$ and $15/2^- \rightarrow 9/2^+$ excitation energies in the $N = 126$ and their neighboring odd- A $N = 127$ isotones. The observed $3^- \rightarrow 0^+$ energy in the present work is marked by red square.

The measured decay strengths deduced from the known lifetimes are given in Table III, where they are compared with the transition strengths calculated using the same shell-model setting as for calculating levels. Effective proton charges are

taken as Ref. [22], which are $1.5e$ for $E2$ transition and $2.4e$ for $E3$ transition, respectively. On the whole, the measured and calculated $E2$ strengths are in reasonable accord. The strength of the $8_1^+ \rightarrow 6_1^+$ transition is $0.115(6)$ W.u. compared to the calculated value of 0.25 W.u. The 12_1^+ and 14_1^+ states are mostly dominated by the $\pi h_{9/2}^4$ and $\pi h_{9/2}^3 f_{7/2}$, respectively. The $E2$ transition connecting them is inhibited by the different configuration with a very weak $B(E2)$ value $0.032(8)$ W.u., while with the same dominant configuration, $B(E2)$ value between 14_1^+ and 12_2^+ is rather strong. The present shell model calculation reasonably predicts the very weak strength. The strong $11_1^- \rightarrow 8_2^+$ and $17_1^- \rightarrow 14_1^+$ $E3$ transitions are consistent with the main single-particle transition $i_{13/2} \rightarrow f_{7/2}$. The strengths of these transitions are comparable to several other nonspin flip $E3$ transitions in this region and to the strength of the $E3$ transition from the octupole state in ^{208}Pb ; while the $11_1^- \rightarrow 8_1^+$ transition instead of the type $i_{13/2} \rightarrow h_{9/2}$ and is slowed down by spin flip. However, the coupling with the 3^- octupole phonon may not be exactly described in the present model space, the $E3$ transitions are necessarily underestimated.

For those new levels which were observed to branch, Table III also gives the γ -intensity branching ratios and the corresponding transition strengths. These ratios, deduced from the data in Table I, are often used for the determination of

TABLE III. Branching ratios and transition strengths in ^{212}Rn .

E_x (keV)	Initial state	Final state	E_γ (keV)	γ branching intensities ^a	Mult. (exp.)	Transition strengths (W.u.)		
						Exp. ^b	Cal.	
						M1	E2	E3
1501.3	4_1^+	2_1^+	227.6		$E2$	1.04(4)	1.46	
1639.5	6_1^+	4_1^+	138.2		$E2$	0.40(5)	0.80	
1639.7	8_1^+	6_1^+	54.2		$E2$	0.115(6)	0.25	
2171.7	6_2^+	4_1^+	670.4	24(6)	$E2$		0.12	
	6_2^+	6_1^+	532.2	76(17)	$E2$		0.28	
2305.6	5_1^+	4_1^+	804.3	85(35)	$(M1 + E2)$		0.09	
	5_1^+	6_1^+	666.0	15(6)	$(M1 + E2)$	<0.01	<0.01	
	5_1^+	6_2^+	133.7	<5	$(M1 + E2)$	0.35	0.28	
2313.5	7_1^+	6_1^+	674.0	20(7)	$(M1 + E2)$		0.05	
	7_1^+	8_2^+	197.3	80(27)	$(M1 + E2)$	0.13	0.66	
	7_1^+	6_2^+	141.8	<7	$(M1 + E2)$	0.19	0.25	
2324.3	4_2^+	2_1^+	1050.9	19(7)	$E2$		5.81	
	4_2^+	4_1^+	823.0	57(21)	$E2$		2.00	
	4_2^+	6_1^+	684.9	24(9)	$E2$		2.65	
	4_2^+	6_2^+	152.4	<5	$E2$		0.45	
2760.3	11_1^-	8_2^+	644.4		$E3$	<35.9 ^c		18.20
	11_1^-	8_1^+	1067.1		$E3$	1.36(17) ^c		0.58
2880.8	12_1^+	10_1^+	226.3		$E2$	4.4(2)	3.51	
3357.0	14_1^+	12_1^+	476.2		$E2$	0.032(8)	0.01	
	14_1^+	12_2^+	59.8		$E2$	<4	3.32	
3686.4	12_3^+	10_1^+	1031.9	33(9)	$E2$		0.04	
	12_3^+	12_1^+	806.1	67(18)	$E2$		0.22	
4065.9	17_1^-	14_1^+	708.7		$E3$	16(6)		18.89
	17_1^-	15_1^-	75.6		$E2$	3.0(16)	2.79	

^aThe relative intensities calculated from all γ -transitions depopulating a level in Table I.

^bFrom Ref. [15] except for the 11_1^- level.

^cThe transition strength deduced from the branching ratio in the present work.

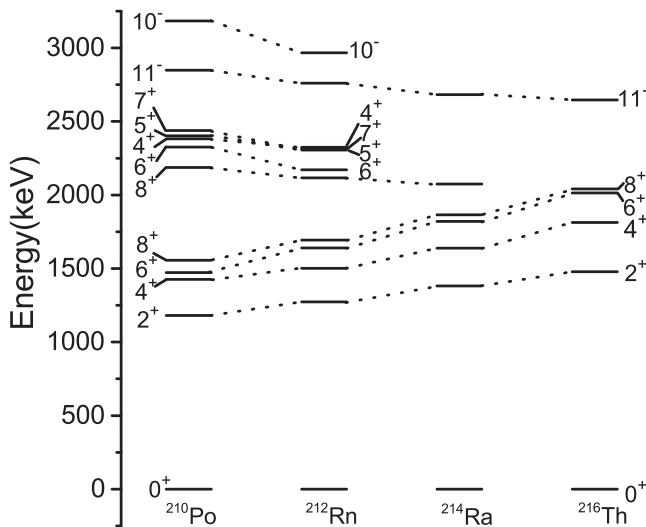


FIG. 7. Systematic behavior of some selected low- and medium-spin levels in ^{210}Po , ^{212}Rn , ^{214}Ra , and ^{216}Th isotones with the $N = 126$.

transition multiplicities and level spins and parities, notwithstanding quantitative agreement with experimental transition branchings was not very good. For example, low-energy intramultiplet transitions between members of the $\pi h_{9/2}^3 f_{7/2}$ multiplet are predicted to compete favorably with the more energetic transitions to levels of the $\pi h_{9/2}^4$ multiplet. Our findings of the 134, 142, and 197 keV transitions as $\pi h_{9/2}^3 f_{7/2}$ intramultiplet transitions are supported by these results and the experimental multiplicities are consistent with the theoretical predictions. However, there is still a need for further experiments to obtain spin and parity assignments, since some of the known spins are only tentative and our experimental setup offered no possibility to analyze angular distribution and conversion-electron.

Figure 7 illustrates the energy level systematics of the even $N = 126$ isotones ^{210}Po , ^{212}Rn , ^{214}Ra , and ^{216}Th . States with the same spin-parity are connected by dot lines. In ^{212}Rn , the spin-parity assignment for the 2967 keV state, which was tentatively assigned as 12^+ in Ref. [9], is instead suggested to be (10^-) , thus allowing its identification as the analog of the 10^- state in neighboring Rn isotopes as mentioned above. The 2_1^+ , 4_1^+ , 6_1^+ , and 8_1^+ states indicate a steady increase energy as proton number increases, while energies for 8_2^+ and 11_1^-

states in Fig. 7 are observed to decrease gradually. These evolutionary tracks could be analyzed in terms of a pairing approach [22,25]. Unfortunately, the study of such a whole systematics from ^{210}Po to ^{216}Th is difficult experimentally because of the inaccessibility of many of the nuclei, especially for the nonyrast and odd-spin yrast states, but they will be of considerable interest in evaluating the development of pairings in the future.

IV. SUMMARY

This work has been successful in identifying many new states in ^{212}Rn above and below the previously identified microsecond isomers. Among the new states, a candidate for the $3^{(-)}$ collective state is suggested. Large-scale shell model calculations are employed to interpret the new established level scheme. The overall agreement between the experimental and theoretical excitation energies, transition strengths is good. According to the calculations, $\pi h_{9/2}^4$ and $\pi h_{9/2}^3 f_{7/2}$ configurations appear to dominate the new assignment of the lowest 5^+ and 7^+ , nonyrast 4^+ , 6^+ , and 8^+ levels, some evidences for $f_{7/2}$ orbitals contribution are observed, in the formation of low-lying 6_5^+ state and high-spin secondary 14_2^+ state. The $3^{(-)}$ state at the excitation energy of 2121 keV has been proposed to originate from the mixing octupole vibration with the 3^- member of the $\pi h_{9/2}^3 i_{13/2}$ multiplet. Further experimental and theoretical investigations would be valuable to confirm the 3^- core-excited state and to study the core-excited structures in ^{212}Rn .

ACKNOWLEDGMENTS

The authors are grateful to the INFN-LNL staff for providing stable ^6Li beam throughout the experiment. This work is supported by the National Nature Science Foundation of China under Grants No. U1832130, No. 11975040, No. 11475013, No. 11975315, No. U1932209, No. 11790322, No. 11775316, No. 11605114, No. 11575118, and No. 11475115; supported by the NSFC-CNNC Joint Project for Nuclear Technology Innovation under Grant No. U1867210; supported by the Continuous Basic Scientific Research Project (Grant No. WDJC-2019-13); supported by China National Nuclear Corporation (Grant No. FA18000201); supported by National Key R&D Program of China (Grant No. 2017YFF0106501); and supported by National Natural Science Foundation of Guangdong, China (Grant No. 2016A030310042).

[1] E. Caurier, G. Martínez-Pinedo, F. Nowacki, A. Poves, and A. P. Zuker, *Rev. Mod. Phys.* **77**, 427 (2005).
 [2] C. Yuan, *JPS Conf. Proc.* **23**, 012026 (2018).
 [3] D. Horn, O. Häusser, T. Faestermann, A. B. McDonald, T. K. Alexander, J. R. Beene, and C. J. Herrlander, *Phys. Rev. Lett.* **39**, 389 (1977).
 [4] D. Horn, O. Häusser, B. Hass, T. K. Alexander, T. Faestermann, H. R. Andrews, and D. Ward, *Nucl. Phys. A* **317**, 520 (1979).
 [5] A. E. Stuchbery, G. D. Dracoulis, A. P. Byrne, and A. R. Poletti, *Nucl. Phys. A* **486**, 397 (1988).

[6] T. Lönnroth, C. W. Beausang, D. B. Fossan, L. Hildingsson, W. F. Piel, Jr., and E. K. Warburton, *Phys. Scr.* **39**, 56 (1989).
 [7] G. D. Dracoulis, P. M. Davidson, A. P. Byrne, B. Fabricius, T. Kibédi, A. M. Baxter, A. E. Stuchbery, A. R. Poletti, and K. J. Schiffer, *Phys. Lett. B* **246**, 31 (1990).
 [8] G. D. Dracoulis, G. J. Lane, A. P. Byrne, P. M. Davidson, T. Kibédi, P. Nieminen, K. H. Maier, H. Watanabe, and A. N. Wilson, *Phys. Lett. B* **662**, 19 (2008).
 [9] G. D. Dracoulis, G. J. Lane, A. P. Byrne, P. M. Davidson, T. Kibédi, P. H. Nieminen, H. Watanabe, A. N.

- Wilson, H. L. Liu, and F. R. Xu, *Phys. Rev. C* **80**, 054320 (2009).
- [10] W. Witthuhn, O. Häusser, D. B. Fossan, A. B. McDonald, and A. Olin, *Nucl. Phys. A* **238**, 141 (1975).
- [11] O. Häusser, T. K. Alexander, J. R. Beene, E. D. Earle, A. B. McDonald, F. C. Khanna, and I. S. Towner, *Hyperfine Interact.* **2**, 334 (1976).
- [12] O. Häusser, J. R. Beene, T. Faestermann, T. K. Alexander, D. Horn, A. B. McDonald, and A. J. Ferguson, *Hyperfine Interact.* **4**, 219 (1978).
- [13] S. J. Poletti, G. D. Dracoulis, A. R. Poletti, A. P. Byrne, A. E. Stuchbery, and J. Gerl, *Nucl. Phys. A* **448**, 189 (1986).
- [14] F. Rösel, H. M. Fries, K. Alder, and H. C. Pauli, *At. Data Nucl. Data Tables* **21**, 291 (1978).
- [15] E. Browne, *Nucl. Data Sheets* **104**, 427 (2005).
- [16] K. Hauschild *et al.*, *Phys. Rev. Lett.* **87**, 072501 (2001).
- [17] L. G. Mann, K. H. Maier, A. Aprahamian, J. A. Becker, D. J. Decman, E. A. Henry, R. A. Meyer, N. Roy, W. Stöfl, and G. L. Struble, *Phys. Rev. C* **38**, 74 (1988).
- [18] W. J. Triggs, A. R. Poletti, G. D. Dracoulis, C. Fahlander, and A. P. Byrne, *Nucl. Phys. A* **395**, 274 (1983).
- [19] E. K. Warburton and B. A. Brown, *Phys. Rev. C* **43**, 602 (1991).
- [20] E. K. Warburton, *Phys. Rev. C* **44**, 233 (1991).
- [21] L. Coraggio, A. Covello, A. Gargano, N. Itaco, and T. T. S. Kuo, *Phys. Rev. C* **60**, 064306 (1999).
- [22] E. Caurier, M. Rejmund, and H. Grawe, *Phys. Rev. C* **67**, 054310 (2003).
- [23] C. Ellegard, P. D. Barnes, E. R. Flynn, and G. J. Igo, *Nucl. Phys. A* **162**, 1 (1971).
- [24] G. D. Dracoulis *et al.*, *Nucl. Phys. A* **493**, 145 (1989).
- [25] D. J. Decman *et al.*, *Z. Phys. A* **310**, 55 (1983).